Available online at www.sciencedirect.com
SCIENCE DIRECT®
Surface Science 559 (2004) 47–62
SURFACE SCIENCE
www.elsevier.com/locate/susc

Atomistic mechanisms for the ordered growth of Co nanodots on Au(7 8 8): a comparison between VT-STM experiments and multi-scaled calculations

S. Rohart [a,*], G. Baudot [a], V. Repain [a], Y. Girard [a], S. Rousset [a,*], H. Bulou [b], C. Goyhenex [b], L. Proville [c]

[a] Groupe de Physique des Solides, Matériaux et Phénomènes Quantiques, Universités Paris 6 et 7, CNRS, UMR 75-88, FR 2437, 2 place Jussieu, 75251 Paris Cedex, France
[b] Institut de Physique et Chimie des Matériaux de Strasbourg, UMR 75-04, 23 rue du Loess, 67037 Strasbourg, France
[c] Service de Recherches de Métallurgie Physique CEA/Saclay, 91191 Gif sur Yvette Cedex, France

Received 30 January 2004; accepted for publication 30 March 2004
Available online 15 April 2004

Abstract

Hetero-epitaxial growth on a strain-relief vicinal patterned substrate has revealed unprecedented 2D long range ordered growth of uniform cobalt nanostructures. The morphology of a sub-monolayer Co deposit on a Au(1 1 1) reconstructed vicinal surface is determined by using variable temperature scanning tunneling microscopy (VT-STM). A rectangular array of nanodots (3.8 nm × 7.2 nm) is found for a particularly large deposit temperature range lying from 65 to 300 K. This paper focuses on the early stage of growth at temperatures between 35 and 480 K. Atomistic mechanisms leading to the nanodots array are elucidated by comparing statistical analysis of VT-STM images with multi-scaled numerical calculations. Molecular dynamics allows the quantitative determination of the activation energies for the atomic motion, whereas the kinetic Monte Carlo method simulates the submonolayer Co growth over mesoscopic time scale and space scale.

Keywords: Cobalt; Gold; Growth; Surface diffusion; Vicinal single crystal surfaces; Molecular dynamics; Monte Carlo simulations; Scanning tunneling microscopy

1. Introduction

Nucleation and growth of mono-disperse nanostructures is a challenging field both for theoretical modeling and practical applications due to their new magnetic, electric and catalytic properties. Growth of regular islands has been achieved in various systems such as metal aggregates supported

* Corresponding authors. Tel.: +33-1-44274673; fax: +33-1-43542878.
E-mail addresses: rohart@gps.jussieu.fr (S. Rohart), rousset@gps.jussieu.fr (S. Rousset).
URL: http://ufrphy.lbhp.jussieu.fr/nano/.

0039-6028/$ - see front matter © 2004 Elsevier B.V. All rights reserved.
doi:10.1016/j.susc.2004.03.064

on insulator surfaces [1,2], hetero-epitaxial growth of semiconductors including self-assembled quantum dots [3,4], and metal on metals systems [5,6]. Although nucleation and growth models have been extensively developed and compared with experiments in the case of homogeneous substrates, growth on heterogeneous substrates has been considered only recently. The hetero-epitaxial growth of highly strain islands is still very difficult to modelize, but simpler systems have been considered such as nucleation on substrates containing point-defects traps [1,2,7] or spatial ordering of islands grown on patterned substrates [6,8]. The use of spontaneously nanostructured substrates as templates for organized growth is a promising way since it allows to grow not only regular nanostructures but also high density nanostructures over macroscopic scales. This opens up new studies of both individual and collective physical properties by means of standard averaging techniques.

Metal on metal growth provides model systems for ordered growth on well-defined nano-patterned substrates [5,6,9]. Experimentally, this phenomenon has been successfully applied to the formation of nanostructures. However, few studies concentrate on the atomistic mechanisms and the quantitative determination of the corresponding energies. The precise determination of the atomistic mechanisms for a given substrate should allow to make prediction in order to get an ordered growth with various deposited materials and to find out the conditions (flux, temperature) for achieving the narrowest size distribution. Indeed the use of a nanostructured template is not sufficient to obtain an ordered growth. For example, the reason why Fe, Co, Ni, Cu [5,10–12] display an ordered growth on Au(1 1 1) at room temperature whereas Ag, Al [12–14] do not is still under debate.

In this paper we study the nucleation and growth of Co nanodots on a Au(1 1 1) reconstructed, vicinal substrate. This system has been shown recently [15–17] to display an improved long-range order and a narrower size distribution than on Au(1 1 1). Using a variable temperature scanning tunneling microscope (VT-STM), we have extensively studied the detailed growth morphology as a function of substrate temperature deposition. A statistical analysis of the STM images has been combined with kinetic Monte Carlo (KMC) simulation and quenched molecular dynamics (QMD) calculation. This enables to elucidate the mechanisms responsible for the organized growth of Co nanodots on Au(7 8 8). Furthermore, this result allows to make quantitative predictions for the ordered growth of other materials on Au(7 8 8) like Fe or Ni.

2. Experimental details

The Au(7 8 8) substrate is a stable, vicinal surface misoriented by 3.5° with respect to the (1 1 1) plane toward the [−2 1 1] azimuth. It has been fully presented in a previous paper [15]. The surface displays a highly regular succession of monoatomic steps and 3.8 nm wide terraces. Due to the $22 \times \sqrt{3}$ reconstruction of the Au(1 1 1) plane, Au(7 8 8) is also reconstructed in the direction perpendicular to the steps (7.2 nm periodicity). It is worth to note the importance of the step direction. Indeed, due to the interaction of the discommensuration line with the step, only vicinal surfaces with {1 1 1}-steps (toward the [−2 1 1] azimuth) display such a pattern [18]. For other step direction different pattern can be expected (for example, on the Au(12 11 11), more complex pattern have been found [19]). The Au(7 8 8) surface is considered here as a model surface since it was shown in earlier studies that it can be used as a template for the growth of cobalt nanodots [15–18]. Indeed, the crossing of a discommensuration line and a step edge acts as a preferred nucleation site.

Our Au(7 8 8) sample is a Au single crystal cut by spark erosion in order to produce a 4 mm diameter and 2 mm thick disk. It was prepared in a UHV chamber (base pressure 3×10^{-11} mbar) using repeated cycles of argon sputtering (5×10^{-6} mbar Ar pressure, 1 keV energy) followed by 850 K annealing.

The cobalt is evaporated from a 2 mm diameter cobalt rod directly heated by electron bombardment ($I_{em} = 12$ mA, $HV = 1$ kV). The pressure

during this process is always below 2×10^{-10} mbar. The flux rate is about 0.2 ML per minute. The uncertainty on the absolute cobalt coverage is about 20%. Deposition was achieved directly under the VT-STM in order to image at the deposition temperature. In order to avoid any shadowing effect, the STM tip was retracted before deposition. For temperatures below room temperature, STM images were taken at the growth temperature in order to ensure that no change could be introduced by the annealing process. For deposition temperatures above room temperature, STM images were taken at room temperature. Cooling down the sample will certainly not change the results (cluster density, size distribution and cluster morphology).

3. VT-STM experiments

In order to determine the atomistic mechanisms responsible for the ordered growth of Co on Au(7 8 8), we have performed STM images for different substrate temperatures and Co coverages. In a first part, we describe the STM images for 35–430 K temperatures range. In a second part, we extract mean quantities from a statistical analysis of the images.

3.1. STM images

STM images of Co deposit on Au(7 8 8) at different temperatures are shown in Fig. 1. Depending on temperatures, several regimes are found. First, for low temperature (below 60 K, see Fig. 1a) no order is found: small clusters are randomly dispersed on the surface and the clusters density is very high. The inset of Fig. 1a shows a low Co coverage image, where single Co adatoms can be seen. We can notice that the positions of these adatoms seem not to be influenced by the particular surface structure (steps, discommensuration lines). At 65 K (Fig. 1b), an organization clearly appears. However, many islands are still randomly located on the surface. Above 65 K, the degree of organization increases. However, few changes are seen versus the temperature: the same result is obtained from 95 to 170 K. In the inset of 1c, we can see that dots are located near the crossing of a discommensuration line and a step edge. We call these sites "preferred nucleation sites". As a consequence an array of pairs of dots situated on a rectangular lattice is developed on the surface. This array displays a long range order as there is exactly one dot on every preferred site. Only few defects (missing dot, dot in a non-preferential surface site, etc.) are seen, which shows the high degree of the organization. From 170 to 300 K the order remains but it is not as good as in the previous temperature range and an increasing number of defects (missing dots, coalesced neighboring dots) can be seen. From 200 to 300 K, low Co coverage images show that many Co atoms are place exchanged into the gold surface layer in preferential atomic sites located near the step edges and the discommensuration lines (cf. inset of Fig. 1e). For temperatures above room temperature, it has been shown [15,16] that the order disappears. We can see in Fig. 1f that the growth at 430 K results in few large faceted clusters randomly distributed on the surface.

The size distributions for different substrate temperatures are presented in Fig. 2. These size distributions were obtained with an object processing software on several images (five to ten 60 nm wide STM images i.e. 1000–2000 dots). At low temperature (40 K in Fig. 2a), the size distribution does not show a maximum and the smallest clusters are most often found. For higher temperatures (95 and 135 K, Fig. 2b and c), the size distributions show a maximum. Moreover, in the 95–170 K range, the width at half maximum decreases when temperature increases and rather good mono-disperse size distributions are obtained above 135 K. It is worth to note that annealing at room temperature increases dramatically the quality of the size distribution [15,17]. At 300 K, the size distribution shows that two kinds of dots co-exist on the surface: smaller ones (less than 20 atoms) and larger ones (more than 100 atoms). This is consistent with the fact that STM images (cf. Fig. 1e) display different islands sizes on the surface. This bimodal size distribution will be discussed later within the framework of KMC simulations. We can remark

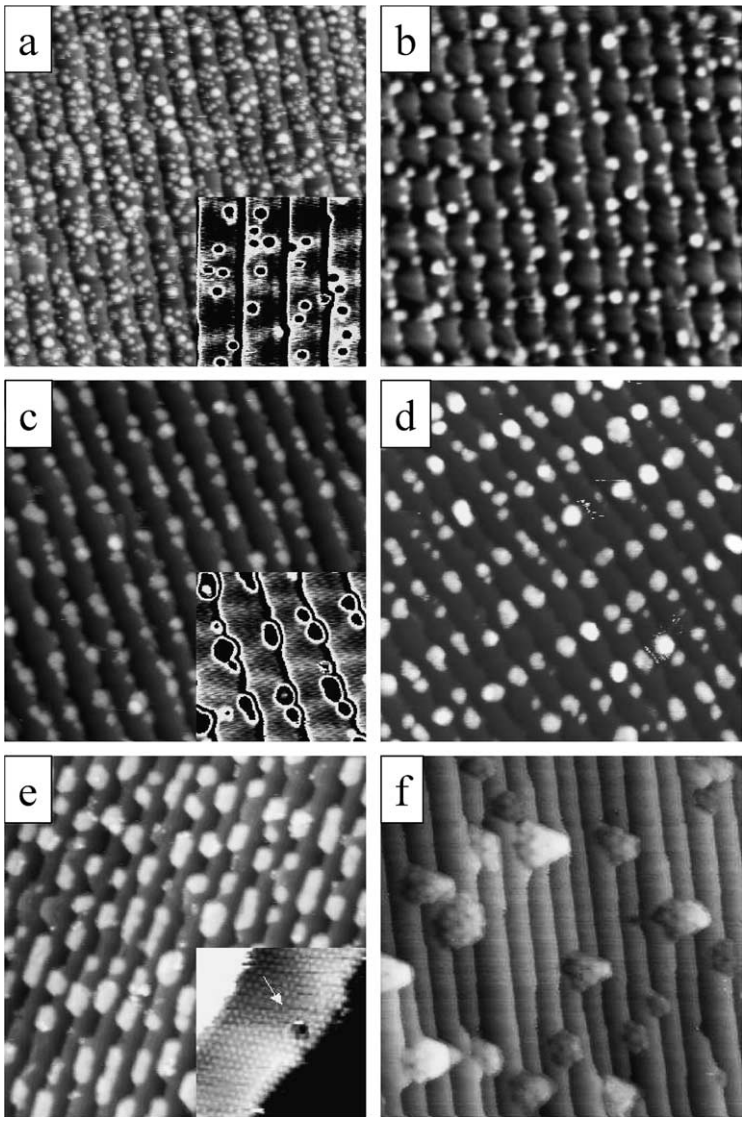

Fig. 1. STM images of cobalt deposition on Au(7 8 8) for different temperatures. (Except for (f) STM images are obtained at the deposition temperature.) Every image is 50 nm wide. (a) $T = 40$ K, $\theta = 0.6$ ML: the dots are randomly distributed on the surface. Inset: 16 nm wide image of 0.005 ML Co on Au(7 8 8). The relief due to the steps has been subtracted in order to enhance the reconstruction corrugation (white lines). (b) 65 K, $\theta = 0.3$ ML: a rough organization is obtained. (c) 95 K, $\theta = 0.3$ ML: a good organization is obtained. Dots are located at the crossing of a discommensuration line and a step edge. Inset: 16 nm wide zoom in of the STM image. The relief due to the steps has been subtracted in order to enhance the reconstruction corrugation. (d) 170 K, $\theta = 0.4$ ML: the good organization in (c) is maintained for temperature up to 170 K. (e) 300 K, $\theta = 0.3$ ML: the organization on the surface disappears and lots of inhomogeneities are seen. Inset: atomically resolved 8 nm wide image which shows a place exchange Co nucleus near the crossing of the discommensuration line and the step edge. This phenomenon has been observed for temperature above 200 K. (f) 430 K, $\theta = 0.4$ ML: the dots are randomly distributed on the surface. This image is taken at room temperature.

that for any temperatures, dots are one or two atomic layers high over the upper step edge and few deviation was found between area and volume distributions.

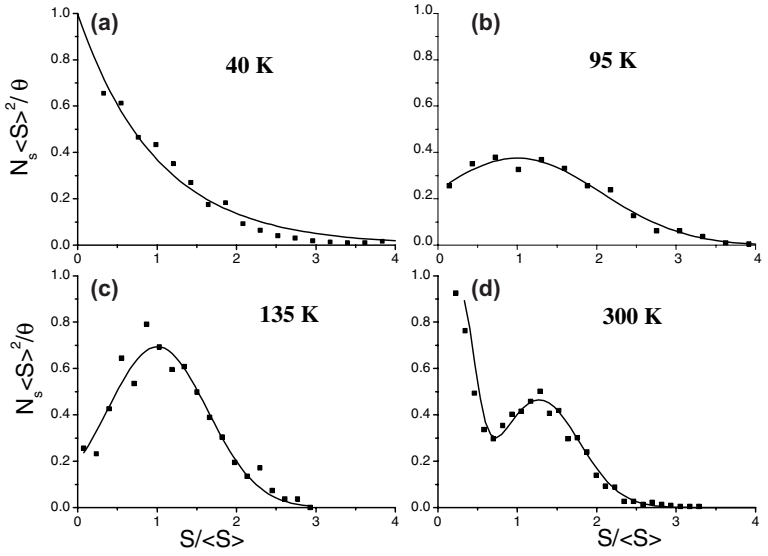

Fig. 2. Normalized size distributions of the Co clusters for different temperatures. (a) $T = 40$ K, $\theta = 0.6$ ML, $\langle S \rangle = 2.8$ Å, fitted by an exponential decay, (b) $T = 95$ K, $\theta = 0.3$, $\langle S \rangle = 6.7$ Å, fitted by a gaussian, (c) $T = 135$ K, $\theta = 0.3$, $\langle S \rangle = 5.3$ Å, fitted by a gaussian and (d) $T = 300$ K, $\theta = 0.3$, $\langle S \rangle = 3.7$ Å, fitted by a combination of a gaussian and an exponential decay.

3.2. Critical cluster density study

UHV VT-STM has been proven to be a powerful technique for quantitative work on nucleation and growth. For each substrate temperature (40–480 K), we have recorded STM images as a function of the cobalt coverage. Analysis of STM images allows to extract the Co clusters density versus the Co coverage. Some of these curves have been plot in Fig. 3. These curves reveal the well-known behavior of sub-monolayer nucleation and growth on surfaces (see for example [20] or [21]). In the nucleation regime, the cluster density increases regularly until the growth regime is reached. Then, the cluster density stabilizes and the cluster size increases. The constant cluster density is called the critical density (n_c). For higher coverage, the coalescence regime starts and the density decreases.

Previous work [20,22–25] has already pointed out the importance of the critical cluster density, in order to elucidate growth mechanisms, since it is related to the diffusion length of adatoms on the surface.

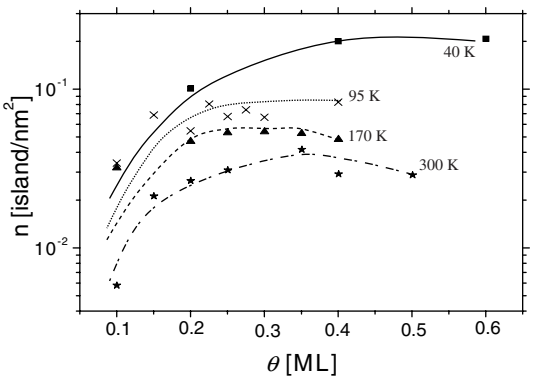

Fig. 3. The cluster density is plotted versus the Co coverage (θ) for different substrate temperatures. The dots are the experimental data and the lines are guides for the eyes.

The experimental behavior of the critical clusters density versus the temperature is given in Fig. 4 in an Arrhenius plot. It displays a large temperature range (60–300 K) where the cluster density is constant. This clearly indicates that the growth is not homogeneous on the Au(7 8 8) surface. This is due to the nano-patterning of the surface. We can remark that the constant density

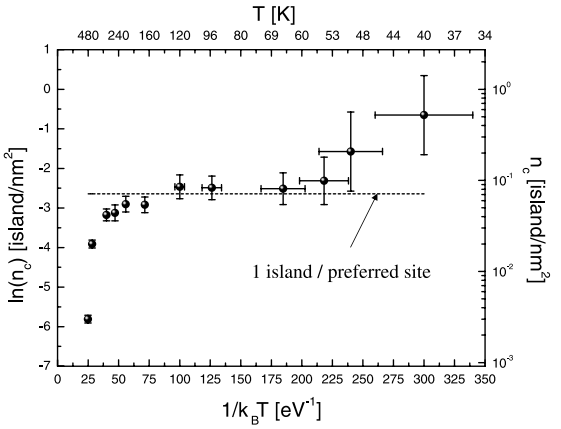

Fig. 4. Arrhenius plot of the critical cluster density versus temperature. The dotted line indicates the density of preferred nucleation sites on Au(7 8 8).

equals the density of preferred nucleation sites. This result is consistent with STM images described above (Fig. 1c and d). The curve clearly shows that the quality of the dots array decreases above 160 K as the clusters density slowly decreases until 300 K as pointed out above. Under 60 K and above 300 K, a strong linear decrease of the clusters density logarithm as a function of $1/k_BT$ is observed, which is characteristic of nucleation and growth on homogeneous surfaces [25]. This indicates that the growth is not governed by the preferred nucleation sites anymore.

4. Interpretation and multi-scaled calculations

We have demonstrated that Co displays an ordered growth on Au(7 8 8) in a large temperature range (65–300 K). As a comparison, one can see that it is particularly larger than the plateau found by Brune et al. [6] for the organized growth of Ag nanodots on Ag bilayer on Pt(1 1 1) (100–130 K). In this case the organized growth was due to a confinement of the adatoms by the dislocation lines of the strain-relief pattern. The organized regime stops as soon as the adatoms have sufficient energy for diffusing across these lines. We want to elucidate what atomistic mechanisms are responsible for the ordered growth on Au(7 8 8), and the observed large temperature range of ordered growth.

4.1. A simple view of the organized growth

What are the relevant parameters for understanding the temperature range of the ordered growth regime?

For low temperatures, the adatoms mean free path on a surface is lower than the mean distance between preferred sites. Indeed, the clusters density is higher than the preferred sites density as it can be seen in Fig. 4. Therefore, the adatoms are not sensitive to the nano-patterning of the surface since the area visited by the adatoms is smaller than the periodic pattern. This explains why no order has been found for the lowest substrate temperatures. Above a temperature threshold (T_o), the system displays an ordered growth. At this temperature, the diffusion length of the adatoms calculated on a homogeneous substrate should equal the distance between preferred sites. As a consequence, the parameters which determine the temperature threshold of the ordered growth regime are the diffusion energy E_{diff} and the distance between preferred nucleation sites l_t (i.e. the density of preferred sites $n_t = 1/l_t^2$).

Using the well-known rate equation (RE) model for homogeneous growth [22,24–26], we estimate the lowest temperature T_o, for which the ordered growth regime of Co on Au(7 8 8) is reached. We assume that all dimers are stable on the surface (critical cluster size $i^* = 1$), since the dimer cohesion energy is much higher than the thermal energy at low temperature. The critical clusters density versus temperature is given by

$$n_c = \eta(D/\sigma F)^{-1/3} = \eta(D_0/\sigma F)^{-1/3}\exp(E_{diff}/3k_BT) \quad (1)$$

with η a constant prefactor (about 0.25 using the lattice approximation for capture rates [25]), F the deposition rate (flux), D_0 the diffusion pre-factor, σ the size of a lattice site and E_{diff} the diffusion energy. The ordered growth regime is reached when the clusters density equals the density of preferred sites (n_t). Taking $n_c = n_t = 1/200$ the

ratio of preferred sites per atomic sites, $E_{\mathrm{diff}} = 0.12$ eV [27,28], $D_0 = 5.8\times10^{12}$ Å^2/s [29] and $\sigma = 7.2$ Å^2 we find that an ordered growth should be observed for temperatures over 83 K, which is a little higher than the experimental value ($T_{\mathrm{o}}^{\mathrm{STM}} = 65$ K). As we know that the RE model given in equation 1 tends to over estimate the dot density [24], we find that there is a good agreement between this rough calculation and STM experiments.

For temperatures above T_{o}, atoms are trapped into the preferred sites and we observe an ordered growth regime. A characteristic of such a regime is that the critical clusters density is constant as a function of temperature and the cluster density value equals the preferred sites density. Indeed the diffusion length of the adatoms is now limited by the existence of the preferred sites. This ordered growth occurs as long as the typical energies of the trapping mechanisms are sufficient to stabilize adatoms in the preferred sites. We call T_{e} the highest temperature for which an ordered growth is observed. The crucial parameter, which determine T_{e}, is the trap energy E_{t}.

In order to estimate T_{e}, we modify the RE model for homogeneous growth to take into account the favored sites, following the model proposed by Venables [7,30]. Assuming for simplicity that dimers are stable on the surface, the RE for the homogeneous growth describes the behavior of adatoms density n_1 and stable islands density n_x. In this new model, we add an homogeneous distribution of traps described by a trap density n_{t}. We then need to consider the trapped adatoms density $n_{1\mathrm{t}}$ and the trapped stable islands density $n_{x\mathrm{t}}$ (now n_x is the density of stable islands not located at the traps). The fate of trapped adatoms is governed by two terms: the trap capture rate for an adatom $\sigma_1 D n_1 n_{\mathrm{te}}$ and the rate for this atom to jump out of the trap $n_{1\mathrm{t}} v_0 \exp\times(-(E_{\mathrm{t}}+E_{\mathrm{d}})/k_{\mathrm{B}}T)$ [30]. σ_1 is the capture rate of a trap (which is assumed for simplicity to be equal to the capture rate of an adatom), D is the usual diffusion coefficient ($D = D_0 \exp(-E_{\mathrm{diff}}/k_{\mathrm{B}}T)$), n_{te} is the density of empty traps ($n_{\mathrm{te}} = n_{\mathrm{t}} - n_{1\mathrm{t}} - n_{x\mathrm{t}}$), v_0 is the attempt frequency and E_{t} is the trap energy. The four rate equations for the behavior of n_1, $n_{1\mathrm{t}}$, n_x and $n_{x\mathrm{t}}$ have the following forms:

$$\begin{cases} \dfrac{\mathrm{d}n_1}{\mathrm{d}t} = F - \sigma_1 D n_1 (2n_1 + n_{\mathrm{te}} + n_{1\mathrm{t}}) - \sigma_x D n_1 (n_x + n_{x\mathrm{t}}) \\ \qquad\qquad + n_{1\mathrm{t}} v_0 \exp(-(E_{\mathrm{t}}+E_{\mathrm{d}})/k_{\mathrm{B}}T) \\ \dfrac{\mathrm{d}n_{1\mathrm{t}}}{\mathrm{d}t} = \sigma_1 D n_1 (n_{\mathrm{te}} - n_{1\mathrm{t}}) - n_{1\mathrm{t}} v_0 \exp(-(E_{\mathrm{t}}+E_{\mathrm{d}})/k_{\mathrm{B}}T) \\ \dfrac{\mathrm{d}n_x}{\mathrm{d}t} = \sigma_1 D n_1^2 \\ \dfrac{\mathrm{d}n_{x\mathrm{t}}}{\mathrm{d}t} = \sigma_1 D n_1 n_{1\mathrm{t}} \end{cases} \tag{2}$$

A key parameter of these equations is the capture rates for an adatom (σ_1) and a stable cluster (σ_x). The choice for the values has been discussed by Brune in [25]. We take $\sigma_1 = 3$ and $\sigma_x = 7$, which was found to give a good agreement for low coverages. In these equations, we neglect the possibility of direct impingement of a deposited atom onto monomeres or islands. These equations are numerically resolved and they allow us to determine the clusters density variations on the surface. The experimental curve of the clusters density versus the temperature is well-fitted in Fig. 5, taking E_{t} as a free parameter. With $E_{\mathrm{t}} = 0.7$ eV, the model in Eq. (2) reproduces very well the temperature at the end of the plateau which is $T_{\mathrm{e}} \simeq 300$ K. This result is consistent with previous theoretical [7,30] and experimental studies of the growth of Pd

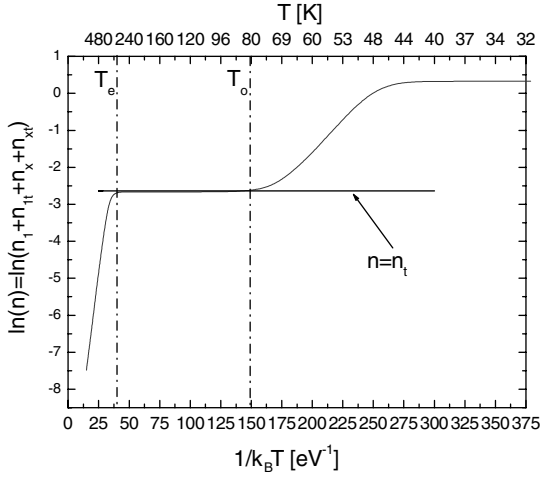

Fig. 5. Rate equation calculation. The model takes into account traps on the surface. The trap energy E_{t} is 0.7 eV in order to fit the experimental data.

on MgO [1] and Fe on CaF_2 [2]. In this work, point defects on the surface trapped the adatoms on the surface and thus lead to a preferred nucleation at the point defects.

This RE calculation gives an estimation of the key parameters involved in the growth of Co on Au(7 8 8). However, in order to go beyond this mean-field approximation, we performed KMC simulations together with QMD calculations for the quantitative determination of the activation energies of the mechanisms involved in the KMC.

4.2. Multi-scaled calculations

4.2.1. Principle of the calculations

The KMC modeling is a powerful tool for studying the nucleation and growth behavior over the time scale of diffusion and for mesoscopic space scale. The reader can refer to the work of Jensen in [21] and Brune in [25] in order to gain more insights into the KMC modeling. The comparison between the STM images and the simulations gives an accurate determination of the atomic mechanisms leading to ordered growth of Co nanodots.

We have developed our own KMC code based on the algorithm of Bortz et al. [31]. The surface is modeled by adsorption sites located at hexagonal lattice sites. Each of this site represents an atomic position where a Co atom may reach a local mechanical equilibrium. The atomic displacements between those sites are ruled by the transition state theory:

$$p_i = v_0 \exp(-\Delta E_i / k_B T) \tag{3}$$

The attempt frequency v_0 is fitted so that the KMC model reproduces the correct diffusion coefficient D_0 given in [29]. We then have $v_0 = D_0/(4\sigma)$ with σ the surface of an atomic site ($\sigma = 2.88 \times 2.88\sqrt{3}/2 = 7.2$ Å^2).

ΔE_i is the energy barrier for the atomic processes. In principle the number of different barriers is very large, and their exact values are unknown. Only approximate total energy methods can at present give results for all the processes of interest here. We have used the quenched-molecular-dynamics (QMD) to give us an idea about the important processes. QMD is an energy minimization procedure, based on the integration of the equation of motion for each atom in the system, which consists of canceling the velocity of the atoms when the product of the force acting on the atoms by their velocity becomes negative. Then, the kinetic energy of the system decreases leading to the minimization of the potential energy at 0 K [32,33]. In our calculations, the equations of motion are integrated with a velocity-Verlet integrator [34] with a time step of 5 fs which is the best compromise between calculation speed and system stability. We considered that the quenched situation is reached when the system temperature is lower than 3 mK with temperature fluctuations lower than 0.2 μK/fs, which ensures an energy accuracy better than 0.1 meV.

The interatomic forces are calculated within the framework of the second moment approximation of the tight binding theory (TBSMA) [35] from the total energy

$$E_{\text{tot}} = \sum_i \left\{ \sum_{j \neq i} A_{X_i Y_j} \exp\left[-p_{X_i Y_j} \left[\frac{r_{ij}}{r_0^{X_i Y_j}} - 1 \right] \right] - \sqrt{\sum_{j \neq i} \xi^2_{X_i Y_j} \exp\left[-2q_{X_i Y_j} \left[\frac{r_{ij}}{r_0^{X_i Y_j}} - 1 \right] \right]} \right\} \tag{4}$$

X and Y indicate the chemical species (Co,Au), r_0^{XX} the first-neighbor distance in the metal X and $r_0^{XY} = \frac{1}{2}(r_0^{XX} + r_0^{YY})$. The parameters A_{XY}, q_{XY}, p_{XY}, and ξ_{XY} (Table 1) are fitted to the experimental values of the cohesive energy, lattice parameter, and elastic constants [36,37] for homoatomic interactions (Co–Co, Au–Au). TBSMA potentials are known to underestimate surface energies. Then, a peculiar attention has been paid in order to reproduce the difference between the surface energies of Co and Au [27]. Heteroatomic interaction Au–Co parameters are calculated by fitting the positive heats of solution for a single substitutional impurities and refined in order to reproduce the existence of a miscibility gap in the phase diagram of the bulk Au–Co system [38].

Calculations have been performed on an Au(1 1 1) slab consisting of two terraces, each of them containing (10 × 15 × 8) gold atoms, plus one

Table 1
Parameter value for Au–Au, Au–Co, and Co–Co interactions

Element	A (eV)	p	ξ (eV)	q	r_0 (Å)
Au–Au	0.189	10.40	1.744	3.87	2.880
Au–Co	0.140	10.63	1.656	3.11	2.695
Co–Co	0.106	10.87	1.597	2.36	2.510

cobalt adatom, with periodic boundary conditions in the directions $\langle 1\,\bar{1}\,0\rangle$ and $\langle \bar{1}\,\bar{1}\,2\rangle$ parallel to the surface. The dimension of the terraces along the $\langle \bar{1}\,\bar{1}\,2\rangle$ has been set in order to reproduce the dimensions of the Au(7 8 8) terraces.

The determination of the relevant processes requires to calculate the activation energy of the different possible mechanisms, i.e. by calculating the energy of the system along the minimum energy path between initial and final states. The problem of finding the minimum energy path for an adatom diffusion from an equilibrium site to another one on simple surfaces, such as Au(1 1 1) for example, is straightforward since it is a straight line between the initial and final states. In the case of more complex surfaces, such as vicinals and reconstructed ones, the problem is more difficult. Near steps and discommensurations, the minimum energy path is no longer a straight line between initial and final equilibrium sites. The most reliable method is then to perform accurate mappings of the adsorption energies of the Co adatom on selected area and then to apply a path finding algorithm.

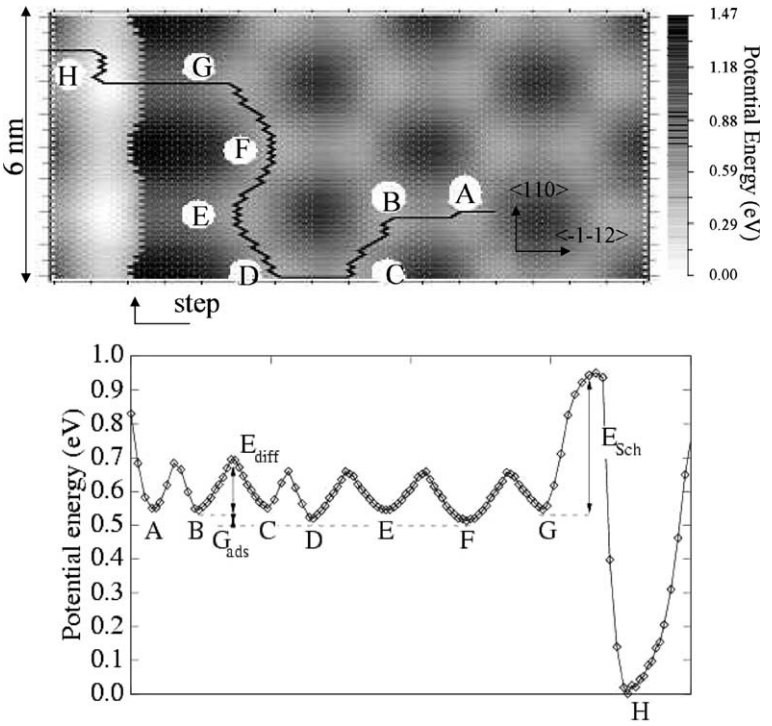

Fig. 6. Energy map of a Co adsorption on Au(7 8 8) near a step. The black line is the minimum energy path from A to H.

Fig. 6 displays the energy map of a Co adsorption in the step area. For each point, only the Co (x, y)-coordinates are strained at fixed values during the quenching procedure. The step of the mappings has been set to 0.100 Å along the $\langle 1\bar{1}0\rangle$ direction and 0.087 Å along the $\langle \bar{1}\bar{1}2\rangle$ direction. The Dijkstra's path finding algorithm has been applied in order to determine the minimum energy path [39].

Searching for simplicity, among numerous events that have been tested by the molecular dynamic, very few of them have been selected for the KMC simulations. The dependence of ΔE_i is represented by $\Delta E_i = E_{\text{diff}} + n \cdot E_{\text{Co–Co}} + \delta_{\text{loc}}$ where n is the number of Co first neighbors. δ_{loc} is zero all over the surface, except for some specific sites where the Co energy landscape is locally modified because of the heterogenities of the substrate. The numerical values of parameters are given in Table 2. The quantity δ_{loc} describes the energies in specific sites and will be given further as ΔG_{ads}, ΔG_{ex}, ΔE_{ex}. The number of atomic events and therefore the number of parameters are reduced to a minimum in order to stress the driving mechanisms. The surface diffusion barrier reported in Fig. 6 ($E_{\text{diff}} = 0.15$ eV) is higher than the one reported in Ref. [27] ($E_{\text{diff}} = 0.12$ eV). The origin of such a discrepancy comes from the fact that in Ref. [27], the calculations have been performed on a $22 \times \sqrt{3}$ reconstructed surface; in this case the stress relief induced by the reconstruction lowers the diffusion energy of adatoms [40–42]. We take $E_{\text{diff}} = 0.12$ eV, which should be more correct for our problem.

For the KMC simulations, the surface is 500×500 sites wide with periodic boundary conditions. The deposition is treated as a random event which has a probability that is adjusted with respect to the deposition rate as suggested in [21].

A KMC simulation with no specific sites, i.e., of a deposition on a virtual homogeneous surface with the parameters of Table 2 is done to compare our KMC model with the RE model for homogeneous nucleation [22,25]. The variation of the critical clusters density with the temperature is shown in Fig. 7. A good agreement has been found for two growth regimes as a function of temperature range.

For the lowest substrate temperatures, the clusters density does not depend on the temperature: this is the "post-nucleation" regime [25] (critical cluster size $i^* = 0$) where the adatoms diffusion is negligible compared to the deposition rate. For higher temperatures, the critical clusters density is given by Eq. (1). This is a regime corresponding to a critical cluster size $i^* = 1$, where the diffusion of adatoms is significant and dimers are stable. Using Eq. (1), a fit of the numerical data from KMC enables us to deduce the diffusion energy. We find 120 ± 2 meV while the input E_{diff} was 120 meV which reveals a good agreement.

For simplicity, the influence of the Schwoebel barriers due to the surface steps on the adatoms diffusion is neglected in our model. This assumption is justified by the fact that the preferred

Table 2
KMC parameters obtained by mean of molecular dynamic calculations

Parameter	Value
v_0	3.28×10^{12} Hz
E_{diff}	0.12 eV
$E_{\text{Co–Co}}$	0.44 eV

The attempt rate v_0 is calculated from Ref. [29] and the diffusion energy E_{diff} can be found in [27,28].

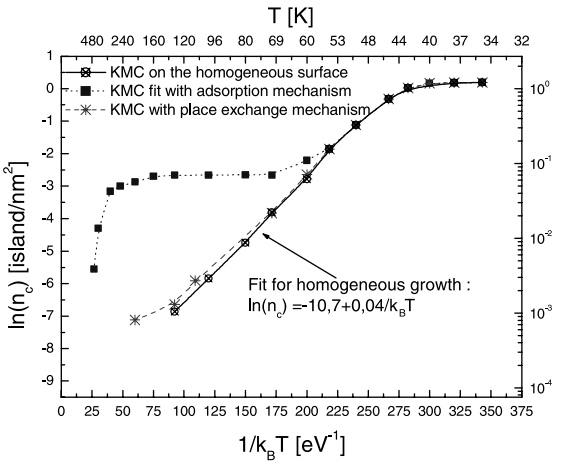

Fig. 7. KMC result for the growth with different models: (⊗) homogeneous surface; (■) surface with preferred site due to preferred adsorption mechanism; (∗) surface with preferred sites due to place exchange mechanism.

adsorption sites decrease the adatoms mean free path. As long as we have an ordered growth, the adatoms mean free path is indeed lower than the terrace width. Thus, nucleation at steps is suppressed since adatoms will reach the preferred adsorption sites first. For higher temperature, i.e. for temperature higher than T_e, the mean free path of adatoms is longer than the terrace width. As a consequence, neglecting the presence of the steps will not gives a good description of the real system for temperatures above T_e. The temperature threshold above which the steps are expected to play a role has been estimated by performing a KMC simulation with a model surface whose steps are considered by infinite Schwoebel barriers. It was found that the temperature threshold is higher than T_e which indicates that our approximation is valid in order to give a good description of the ordered growth regime.

The effect of the discommensuration lines is simplified by introducing a set of preferred sites on the KMC model surface. Each preferred sites is located near the step edge (the possibility of a repulsive diffusion barrier to cross the discommensuration line as suggested in [27] is neglected). According to the atomically resolved STM images [15] of the Au(7 8 8) structure, which show place exchange Co atoms into the gold surface layer, two preferred sites are separated by seven atomic sites in the $\langle 1\,1\,0\rangle$ direction and the density of the preferred sites is 1/200.

In the nucleation preferred sites, two different mechanisms are investigated: (i) a preferred adsorption mechanism, which was predicted by QMD calculations on the reconstructed Au(1 1 1) surface in [27]; (ii) a place exchange mechanism of the adsorbed Co atom located on top of the underlying Au atoms, since this site was observed by atomically resolved STM [15]. The preferred adsorption mechanism involves only one additional parameter compared with the case of homogeneous surface growth: the adatom energy gain in the preferred site is ΔG_{ads} measured with respect to the usual adsorption site (see position 3 in Fig. 8a). The exchange mechanism is described with two additional parameters: the activation barrier for the exchange ΔE_{ex} and the energy gain of the atom ΔG_{ex} when it is inserted into the gold surface layer (see position 4 in Fig. 8a). The three additional parameters have been estimated by QMD calculations. Fig. 8b displays the minimum energy path for a Co–Au exchange near the step. Only the Co z-coordinate has been strained during the quenching procedure.

4.2.2. Atomistic mechanisms for the ordered growth

In order to prove that both mechanisms described above are necessary here, we perform successively the KMC simulations with one mechanism only.

We first report a KMC simulation with the preferred adsorption mechanism only. The best fit to the experimental curve showing the maximum clusters density versus the temperature leads to $\Delta G_{ads} = 0.7$ eV (see Fig. 7). A qualitative agreement between the experiment and the KMC simulations is found. This simulation is very close to the RE calculation described above as they both correspond to the same mechanism. This fit is obtained by using the same energy barrier to leave the preferred site ($\Delta G_{ads}^{KMC} + E_{diff} = E_t + E_{diff} = 0.82$ eV) in both KMC and RE calculation. It is worth to note that the fit for low temperatures is better with KMC than with the RE model. The temperature T_o is particularly well reproduced with this model ($T_o^{KMC} \simeq 75$ K, $T_o^{STM} \simeq 70$ K). The end of the plateau is much better reproduced by KMC than by RE calculation. This is due to the influence of the dimer bonds: in RE calculation the possibility for a dimer to break is neglected although the dimer binding energy (0.52 eV) is small with respect to the temperatures at the end of the plateau (about $T = 300$ K).

The value of $\Delta G_{ads} = 0.7$ eV, which is close to 1 eV is in agreement with what has been found in the literature for nucleation at defect sites with a high trapping energy [1,2]. However, the difference in this study is that we know the possible nucleation mechanisms. This leads us to remark that the value of $\Delta G_{ads} = 0.7$ eV cannot represent a preferred adsorption mechanism. For example, this value is in strong contradiction with the QMD calculations, which indicates a value of 0.1 eV [27] on a flat reconstructed surface. Although the presence of the step is not included in the QMD calculation of [27], the correction is not expected to be so

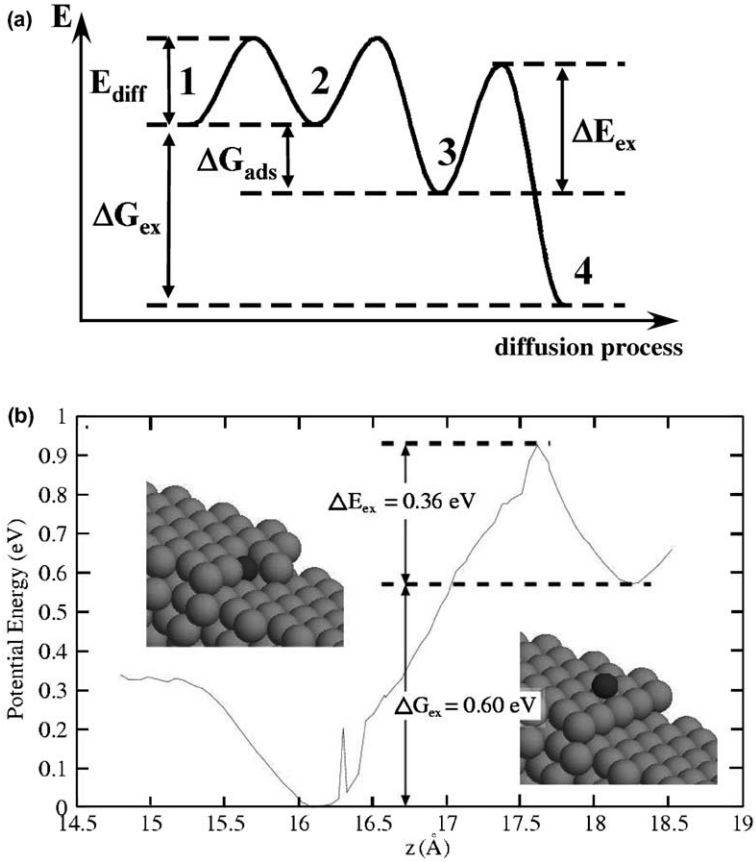

Fig. 8. (a) Energetic models used in the KMC simulations for the mechanisms in the preferred sites: the adatom diffuses from simple sites (1 and 2) to the preferred sites (3 and 4). The atom first gains an adsorption energy ΔG_{ads} (3) with respect to the simple sites. Then it can exchange with a gold atom (4) by jumping over the exchange barrier ΔE_{ex}. The energy gain compared to a simple site is ΔG_{ex}. (b) QMD calculation for the place exchange mechanism at the step edge.

large. Such a value should correspond to a more complex mechanism, such as a place exchange one, which is investigated below.

Now, we consider a KMC simulation with the preferred place-exchange mechanism only. In this simulation, we used the following energy parameters. Taking into account both results with RE calculation and previous KMC simulation, we set the energy to leave the preferred site to 0.82 eV. We add an energy barrier to reach the preferred site $\Delta E_{ex} = 0.32$ eV so that the place exchange mechanism is very efficient above 200 K according to the VT-STM experiments. The gain of the Co atom when it is inserted is thus $\Delta G_{ex} = 0.5$ eV. The result of this simulation is displayed in Fig. 7. The KMC curve taking into account the exchange mechanism only is very similar to the curve obtained for homogeneous growth. Indeed, within the explored temperature range, only very few deviation of the homogeneous growth regime is clearly seen (see Fig. 7). The small deviation appearing at about 150 K can be explained by the activation of the preferred place exchange mechanism. The disagreement with the experimental data can be understood as follows: when the adatoms have sufficient energy in order to diffuse along a distance equal to the distance between preferred sites, the energy barrier ΔE_{ex} prevent

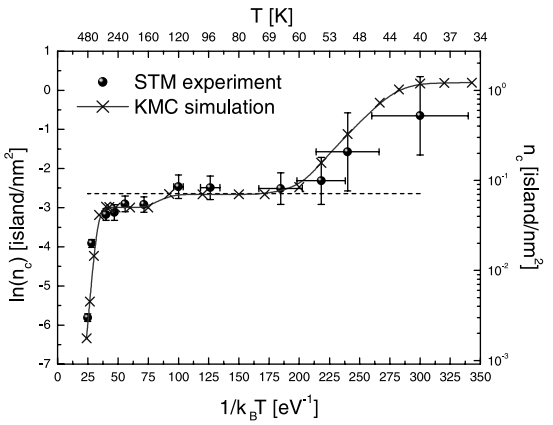

Fig. 9. KMC simulation of the growth of Co nanodots on Au(7 8 8). A good fit of the experimental data for the critical clusters density versus the temperature is obtained with a model combining both the adsorption and place exchange mechanisms in the preferred sites.

them from reaching the preferred site, (we can remark that this value is very low in comparison to typical values for the place exchange on a flat, unreconstructed surface). As a consequence, the critical cluster density keeps on decreasing as the preferred sites cannot play any role. When the thermal energy of the adatoms is higher than the place exchange barrier, the nucleation becomes heterogeneous but there is still less than one dot per preferred site. We can conclude that the preferred place exchange mechanism cannot explain alone the experimental results. This is consistent with the low coverage images for various temperatures which do not show the place exchange mechanism below 200 K.

4.3. Interplay between adsorption and place exchange mechanisms

A good fit of the experimental data is achieved with the combination of both mechanisms in the preferred sites (see Fig. 9). Realistic parameters used in this fit are summarized in the Table 3. For this simulation we still have $\Delta E_{ex} = 0.32$ eV, which ensures that no place exchange occurs before 200 K. The energy to leave the preferred sites (removal process for the place exchange) is still 0.82 eV ($\Delta G_{ex} + \Delta E_{ex} - \Delta G_{ads}$, see Fig. 8). This table gives also parameters obtained by QMD. These parameters are calculated on various surfaces—non-reconstructed Au(7 8 8) and reconstructed Au(1 1 1)—as we do not precisely know the atomic structure of the Au(7 8 8) surface. This allows us to make a comparison with the parameters found in KMC calculations. The adsorption gain ΔG_{ads} was found to be 0.28 eV in KMC. This high value with respect to the QMD on the discommensuration line on Au(1 1 1) might be due to the influence of the step edge. Indeed, for the discommensuration line on the Au(1 1 1) surface, every sites along the line is equivalent. This is not the case on the Au(7 8 8) surface which indicates that the step edge changes the adsorption energies and induces a more favorable site near the step edge. The values found by the QMD for the exchange mechanism are of the same order of magnitude as the values of the KMC although the discommensuration lines are not included in this calculation. The reason why the exchange takes place at a precise site is due to kinetic effects. Indeed the exchange and the preferred adsorption take place at the same

Table 3
KMC parameters for the preferred adsorption and the exchange mechanisms used in order to fit the experimental data

Parameter	KMC	Molecular dynamic	
		Au(7 8 8) non-reconstructed	Au(1 1 1) non-reconstructed
E_{diff}	0.12 eV	0.15 eV	0.12 eV
ΔG_{ads}	0.28 eV		0.10 eV
ΔG_{ex}	0.78 eV	0.60 eV	
ΔE_{ex}	0.32 eV	0.36 eV	

For comparison, various QMD parameters are given. Calculations were done on a Au(7 8 8) non-reconstructed surface and on a Au(1 1 1) reconstructed surface (see [27,43]). The exchange on the Au(7 8 8) surface was located at 1 row away from the step edge. The exchange and adsorption on Au(1 1 1) were performed on top of the discommensuration line.

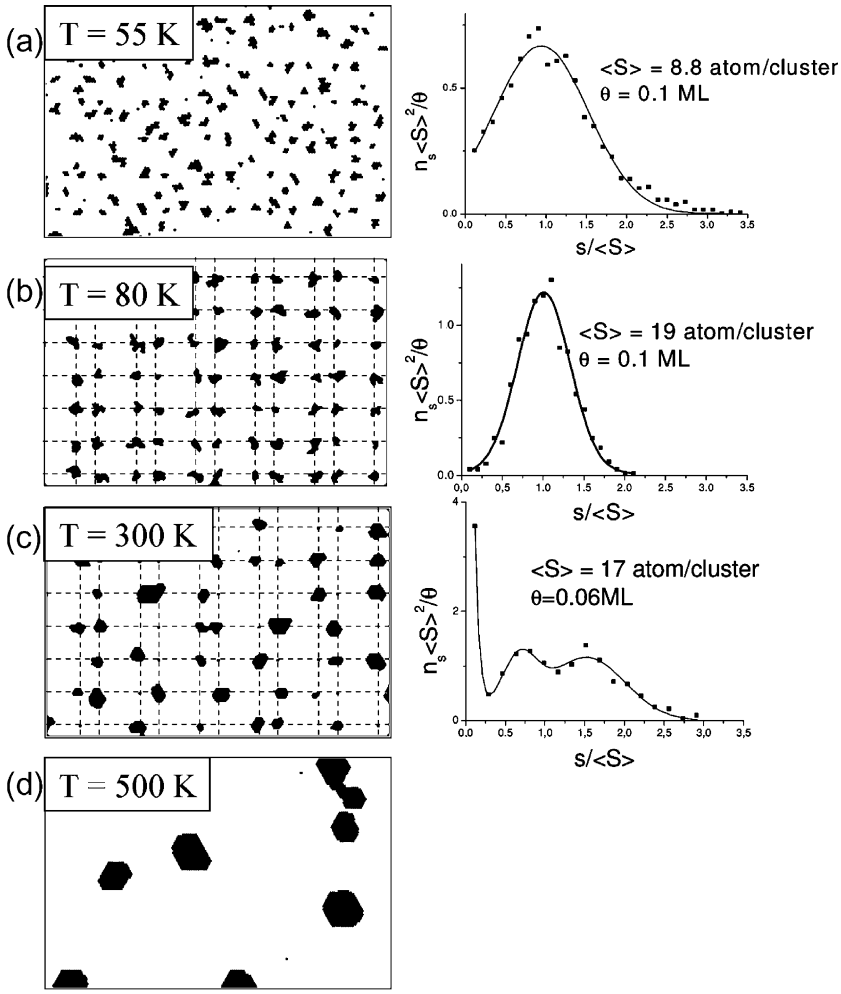

Fig. 10. KMC images and size distributions of the simulation of the growth of Co nanodots on Au(7 8 8). They show a good agreement with STM images. Images are 20×40 nm (a–c) or 50×75 nm (d) wide and are taken at (a) $T = 55$ K, (b) $T = 80$ K, (c) $T = 300$ K and (d) $T = 450$ K.

location. The adsorption gain in this site increases the residence time of the adatoms on this sites which increases the exchange probability in the same way.

In Fig. 9, a plateau with exactly one dot per preferred site is found in the 65–150 K temperature range. Only the preferred adsorption mechanism is able to explain this plateau since we have seen above that no place exchange occurs at such low temperatures. It should be pointed out that the KMC images shown in Fig. 10 are in good agreement with STM experiments. This definitely confirms that the best condition for a long range ordered growth with a narrow cluster size distribution is a sample deposition temperature around 130–150 K.

Above 150 K, the adsorption energy gain is not sufficient anymore in order to stabilize the adatoms. However, the organization is kept due to the activation of the place exchange mechanism. Then a rough organization is maintained up to 300 K, i.e., the number of cluster per preferred sites is between 1 and 2. The most important point, in this temperature range, is that the order still exists on the surface (see Fig. 10c) while the number of defects (empty favored site, coalesced

neighboring dots, etc.) is more important than in the 65–150 K previous regime. This result is particularly clearly seen at $T = 300$ K. At this temperature, the experimental bimodal size distribution is pretty well reproduced. The origin of these inhomogeneities is the weakness of the bonds between the Co atoms: at 300 K, the critical size (largest unstable cluster) of a cluster in a preferred site is 2. This explains why the growth of the dots in the preferred sites is strongly inhomogeneous: some dots grow faster and lead to large clusters when they coalesce with the neighboring clusters.

One question remains: why in the 200–300 K temperature range is there still an organization, whereas in the simulation including only the exchange mechanism with the same parameters is there not any? This may be explained by the fact that the cluster density behavior is not simply due to the sum of both mechanisms but a combination of them. Above 200 K, even if the preferred sites cannot stabilize adatoms by the adsorption mechanism only, the residence time of the adatoms is increased in these sites. As a consequence, the exchange probability is increased in the same way, and the organization may take place.

An important point is the interplay between both mechanisms. This is a key point in order to maintain the organization on such a wide temperature span. The interplay only occurs if the removal process energy of the adsorption ($E_{\text{diff}} + \Delta G_{\text{ads}}$) is higher than the place exchange barrier ΔE_{ex}. In the case of Co on Au(7 8 8) these energies are very close. This explains why the interplay is not perfect and leads to a small accident around 150 K in the curve of the critical clusters density versus temperature (see Fig. 9).

5. Conclusion

The ordered growth of Co nanodots on the Au(7 8 8) surface is proven to be due to the presence of preferred sites. The origin of the preferred sites together with the atomic process responsible for the organization are clearly elucidated. The ordered growth regime occurs on a wide temperature range $[T_o, T_e]$. T_o and T_e are respectively determined by two key energy parameters E_{diff}, the diffusion energy and E_t, the energy to leave the preferred sites. For temperatures below T_o, organization is limited by the adatoms diffusion length. Above T_e, the energy gain in the preferred sites is no more sufficient to stabilize the adatoms and to lead to an ordered array of clusters. The particularity of the organized growth of Co on Au(7 8 8) is that it occurs for a very large temperature range [65, 300 K]. This is explained by a mechanism which combines a strong energy gain with a low activation barrier. In this case, we have identified each mechanism. We found that this can be achieved by an interplay between two mechanisms: adsorption (low activation barrier) and place exchange (high energy gain). The calculations show that the interplay is efficient when the energy gain of the adsorption is higher than the activation energy of the place exchange. Further experiments and calculations for deposition of other materials on other reconstructed surfaces should be of interest to confirm our nucleation and growth scenario.

Acknowledgements

We gratefully acknowledge C. Priester and G. Prévot for the enlightening discussions.

References

[1] G. Haas, A. Menck, H. Brune, J. Barth, J. Venables, K. Kern, Phys. Rev. B 61 (2000) 11105.
[2] K. Heim, S. Coyle, G. Hembree, J. Venables, J. Appl. Phys. 80 (1996) 1161.
[3] J. Tersoff, C. Teichert, M. Lagally, Phys. Rev. Lett. 76 (1996) 1675.
[4] C. Teichert, Phys. Rep. 365 (2002) 335.
[5] D. Chambliss, R. Wilson, S. Chiang, Phys. Rev. Lett. 66 (1991) 1721.
[6] H. Brune, M. Giovannini, K. Bromann, K. Kern, Nature 394 (1998) 451.
[7] J. Venables, P. Bennett, H. Brune, J. Drucker, J.H. Harding, Phil. Trans. R. Soc. Lond. A 361 (2003) 311.
[8] C. Lee, A. Barabàsi, Appl. Phys. Lett. 73 (1998) 2651.
[9] H. Ellmer, V. Repain, M. Sotto, S. Rousset, Surf. Sci. 511 (2002) 183.
[10] B. Voigtländer, G. Meyer, N. Amer, Surf. Sci. 255 (1991) L529.

[11] B. Voigtländer, G. Meyer, N. Amer, Phys. Rev. B 44 (1991) 10354.
[12] H. Bulou, C. Goyhenex, Phys. Rev. B 65 (2001) 45407.
[13] J. Meyer, I. Baikie, E. Kopatzki, R. Behm, Surf. Sci. 365 (1996) L647.
[14] B. Fischer, H. Brune, J. Barth, A. Fricke, K. Kern, Phys. Rev. Lett. 82 (1999) 1732.
[15] V. Repain, G. Baudot, H. Ellmer, S. Rousset, Europhys. Lett. 58 (2002) 730.
[16] V. Repain, G. Baudot, H. Ellmer, S. Rousset, Mater. Sci. Eng. B 96 (2002) 178.
[17] G. Baudot, S. Rohart, V. Repain, H. Ellmer, Y. Girard, S. Rousset, Appl. Surf. Sci. 212–213 (2003) 360.
[18] V. Repain, J. Berroir, S. Rousset, J. Lecoeur, Surf. Sci. 447 (2000) L152.
[19] S. Rousset, V. Repain, G. Baudot, Y. Garreau, J. Lecoeur, J. Phys.: Condens. Matter 15 (2003) S3363.
[20] H. Brune, G. Bales, J. Jacobsen, C. Boragno, K. Kern, Phys. Rev. B 60 (1999) 5991.
[21] P. Jensen, A. Barabàsi, H. Larralde, S. Havlin, H.E. Stanley, Phys. Rev. B 50 (1994) 15316.
[22] J. Venables, Phil. Mag. 17 (1972) 697.
[23] J. Venables, Phys. Rev. B 36 (1987) 8.
[24] M. Bott, M. Hohage, M. Morgenstern, T. Michely, G. Comsa, Phys. Rev. Lett. 76 (1996) 1304.
[25] H. Brune, Surf. Sci. Rep. 31 (1998) 121.
[26] J. Villain, A. Pimpinelli, L.-H. Tang, D. Wolf, J. Phys. I France 2 (1992) 2107.
[27] C. Goyhenex, H. Bulou, Phys. Rev. B 63 (2001) 235404.
[28] Y. Liu, D. Sun, X. Gong, Surf. Sci. 498 (2002) 337.
[29] H. Bulou, O. Lucas, M. Kibaly, C. Goyhenex, Comp. Mater. Sci. 27 (2003) 181.
[30] J. Venables, Physica A 239 (1997) 35.
[31] A. Bortz, M. Kalos, J. Lebowitz, J. Comp. Phys. 17 (1975) 10.
[32] J. Luo, B. Legrand, Phys. Rev. B 38 (1988) 1728.
[33] C. Bennett, in: A.S. Nowick, J.J. Burton (Eds.), Diffusion in Solids, Recent Developments, Academic Press, New York, 1975, p. 73.
[34] W.C. Swope, H.C. Andersen, P.H. Berens, K.R. Wilson, J. Chem. Phys. 76 (1982) 637.
[35] F. Ducastelle, J. Phys. (Paris) 31 (1970) 1055.
[36] G. Simmons, H. Wang, in: Single Crystal Elastic Constants and Calculated Aggregates Properties, MIT, Cambridge, 1971.
[37] C. Kittel, Introduction to Solid State Physics, seventh ed., John Wiley & Sons, New York, 1996.
[38] I. Chado, C. Goyhenex, H. Bulou, J.-P. Bucher, Appl. Surf. Sci. 226 (2004) 178.
[39] E.W. Dijkstra, Numer. Math. 1 (1959) 269.
[40] H. Brune, K. Bromann, H. Röder, K. Kern, J. Jocobsen, P. Stolze, K. Jacobsen, J. Nørskov, Phys. Rev. B 52 (1995) R14380.
[41] C. Ratsch, A. Seitsonen, M. Scheffler, Phys. Rev. B 55 (1997) 6750.
[42] M. Schroeder, D. Wolf, Surf. Sci. 375 (1997) 129.
[43] C. Goyhenex, H. Bulou, J.-P. Deville, G. Tréglia, Appl. Surf. Sci. 188 (2002) 134.